

Generation of density inhomogeneities by magnetohydrodynamic waves in two dimensions

S. Van Loo,¹* S. A. E. G. Falle² and T. W. Hartquist¹

¹*School of Physics and Astronomy, University of Leeds, Leeds LS2 9JT*

²*Department of Applied Mathematics, University of Leeds, Leeds LS2 9JT*

Accepted - . Received - ; in original form -

ABSTRACT

Using two dimensional simulations, we study the formation of structures with a high-density contrast by magnetohydrodynamic waves in regions in which the ratio of thermal to magnetic pressure is small. The initial state is a uniform background perturbed by fast-mode wave. Our most significant result is that dense structures persist for far longer in a two-dimensional simulation than in the one-dimensional case. Once formed, these structures persist as long as the fast-mode amplitude remains high.

Key words: MHD – stars: formation – ISM: clouds.

1 INTRODUCTION

One of the outstanding problems in star formation is the determination of the mechanisms that are responsible for the observed clumpiness in star forming regions. Since the ratio, β , of the thermal to magnetic pressure is observed to be small (Crutcher 1999), it is natural to suppose that magnetohydrodynamic (MHD) waves play a crucial role. For this reason, there have been a number of three-dimensional (3D) simulations of the effect of MHD waves on an isothermal plasma in which β is small (e.g. Ballesteros-Paredes & MacLow 2002; Padaan & Nordlund 2002; Gammie et al. 2003; Li et al. 2004; Nakamura & Li 2005; Vázquez-Semadeni et al. 2005). These do, indeed, show that density inhomogeneities can be formed in this way with statistical properties that are consistent with the observations. However, these calculations generally contain so many ingredients that they obscure the fundamental mechanisms.

In two previous papers (Falle & Hartquist 2002, hereafter FH02 and Lim, Falle & Hartquist 2005, hereafter LFH05), we carried out 1D calculations of MHD waves in a low- β plasma that were designed to elucidate the mechanism by which clumps are formed. In FH02, we showed that clumps with a high-density contrast could be generated by the excitation of slow-mode waves due to the non-linear steepening of a fast-mode wave. In LFH05, we explored how these effects were modified by the dissipation due to ion-neutral friction. The present paper is an extension of the work in FH02 to two dimensions. We find that the mechanism described in the previous paper works even better in

two dimensions in the sense that the density contrasts are both larger and persist for longer.

The governing equations and the initial condition are given in Sect. 2. We then discuss the results for a specific numerical model (Sect. 3) and examine how these depend on the model parameters (Sect. 4). Finally, we conclude the paper by relating our results to observations of clumps and dense cores in GMCs (Sect. 5).

2 NUMERICAL CALCULATIONS

2.1 Governing equations

While FH02 considered only variations in the x -direction, we also allow changes in the y -direction. Since we are only interested in magnetosonic waves, there is no need to introduce a z -component of either the magnetic field or the velocity. The MHD equations for an isothermal gas can then be written in the form

$$\frac{\partial \mathbf{U}}{\partial t} + \frac{\partial \mathbf{F}}{\partial x} + \frac{\partial \mathbf{G}}{\partial y} = 0,$$

where

$$\mathbf{U} = [\rho, \rho v_x, \rho v_y, B_x, B_y]^t$$

is a vector of conserved variables, and

$$\begin{aligned} \mathbf{F} &= [\rho v_x, \rho v_x^2 + p_g + B^2/2 - B_x^2, \rho v_x v_y - B_x B_y, 0, v_x B_y - v_y B_x]^t, \\ \mathbf{G} &= [\rho v_y, \rho v_y v_x - B_y B_x, \rho v_y^2 + p_g + B^2/2 - B_y^2, v_y B_x - v_x B_y, 0]^t, \end{aligned}$$

are the corresponding fluxes. Here we assume that $p_g = \rho a^2$, where a is a constant sound speed. These equations were solved using the second order upwind scheme described in Falle, Komissarov & Joarder (1998), except that we use the divergence cleaning technique described by Dedner et al. (2002).

* E-mail: svenvl@ast.leeds.ac.uk

2.2 Initial state

As in FH02, we are interested in the generation of density inhomogeneities by fast-mode waves propagating in the positive x -direction. Such a wave propagates with speed

$$v_x + c_f,$$

where the fast magnetosonic speed, c_f , is given by

$$c_f^2 = \frac{1}{2} \left[B^2/\rho + a^2 + \sqrt{(B^2/\rho + a^2)^2 - 4a^2 B_x^2/\rho} \right].$$

The form of such a wave is most conveniently written in terms of the primitive variables

$$\mathbf{P} = [\rho, v_x, v_y, B_x, B_y]^t.$$

We then have

$$\frac{\partial \mathbf{P}}{\partial x} \propto \mathbf{r}_f$$

where

$$\mathbf{r}_f = \left(\rho, c_f, -\frac{c_f B_x B_y}{\Delta_f}, 0, \frac{\rho c_f^2 B_y}{\Delta_f} \right)^t \quad \text{with} \quad \Delta_f = \rho c_f^2 - B_x^2.$$

is the right eigenvector for a fast-mode wave propagating in the positive x direction for the system written in terms of the primitive variables, \mathbf{P} . Note that we assume that the fast-mode wave is non-degenerate i.e. neither B_y nor B_x vanish.

Like FH02, we use the above expression to superpose a small amplitude sinusoidal fast-mode wave propagating in the positive x -direction on a uniform background at rest. In order to make the flow two dimensional, we also introduce a shift with respect to the x -axis that depends on y . The initial state is given by

$$\mathbf{P}(x, y, 0) = \mathbf{P}_0 + A_1 \sin \left\{ \frac{2\pi}{L_1} \left[x + A_2 \sin \left(\frac{2\pi y}{L_2} \right) \right] \right\} \mathbf{r}_f, \quad (1)$$

where A_1 and L_1 are the amplitude and wavelength of the fast-mode wave and A_2 and L_2 the amplitude and wavelength of the phase shift. The homogeneous background state \mathbf{P}_0 is as in FH02:

$$\rho = 1, \quad p = T_e \rho, \quad \mathbf{v} = 0, \quad B_x = 1, \quad B_y = \alpha B_x.$$

Here $T_e (= a^2)$ is the equilibrium temperature of the isothermal gas. As in FH02, we use $T_e = 10^{-3}$ (or $a = 0.0316$). Since the amplitude is small, the fast-mode \mathbf{r}_f is calculated using the values of the unperturbed state and is normalised so that the amplitude of v_x is A_1 .

Density inhomogeneities are generated for all values of α . However, the highest contrasts are obtained when the initial wave propagates at a modest angle to the field (FH02). In our calculations we therefore limit ourselves to $\alpha = 0.25$. We set $A_1 = 0.05$ since the transverse magnetic field changes sign for larger amplitudes. The non-linear steepening of the wave then leads to the formation of an intermediate shock, which is unphysical (Falle & Komissarov 2001). We adopt $A_2 = 1$ for the amplitude of the phase shift. Other values for the model parameters are being considered in Sect. 4.

Note that in the initial state, $\mathbf{P}(x, y, 0)$, B_x is constant, while B_y is a function of y . This means that the divergence constraint $\nabla \cdot \mathbf{B} = 0$ is violated. However, for the adopted parameters (see also below), we find that $\nabla \cdot \mathbf{B} < 10^{-5}$, which is of the same order of magnitude as the divergence errors

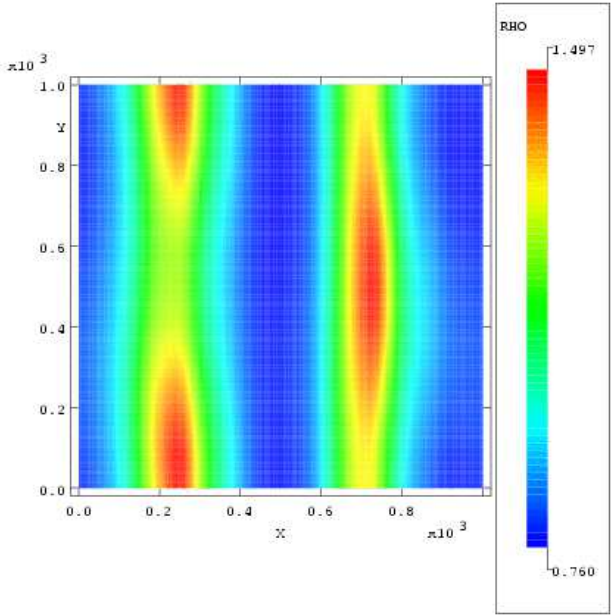


Figure 1. The density at $t = 2000$. The contour lines are added to show that two regions can be distinguished. The central region lies approximately within $250 < y < 750$.

that arise in numerical MHD calculations due to discretisation of the equations. As we include the divergence cleaning algorithm of Dedner et al. (2002) to stabilize the numerical scheme, the initial violation of the divergence constraint is damped out.

Our initial state has an advantage over other models which introduce the two-dimensionality in a more natural way, i.e. a simple y -dependence of the primitive variables that allows an unambiguous interpretation of the initial stages of the simulations. A small density variation or a magnetic field B_x that varies slightly with y introduces a complex y -dependence for the primitive variables (through c_f and Δ_f). Calculations done with these alternative initial states, however, produce similar results to those of our model and hence provide a posteriori justification for our choice.

The computational domain is $0 \leq x \leq L_1$ and $0 \leq y \leq L_2$ ($L_1 = L_2 = L = 1000$) with periodic boundary conditions. We use a uniform grid with 1000×1000 mesh points.

3 RESULTS

Initially the solution is almost one dimensional: the gradients in the y -direction are of the order $L/2\pi A_2 (\approx 100)$ smaller than the gradients in the x -direction. Although these variations are small, they cannot be neglected. From Eq. (1) we see that the gradients in the y -direction change sign when $y = L/4 = 250$ and $y = 3L/4 = 750$ (for any given value of x). This means that the domain can be divided into two regions with different temporal evolution: a central part with $250 < y < 750$ and the rest of the domain. In Fig. 1 we can clearly see these two regions. Note that at this stage the variations in the y direction are of the order of a few percent.

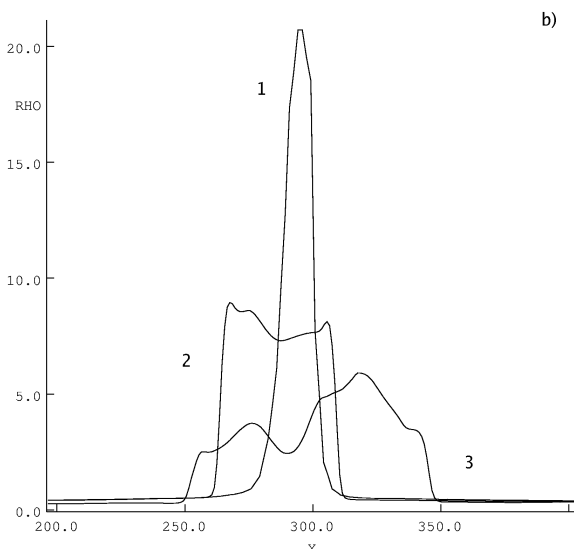
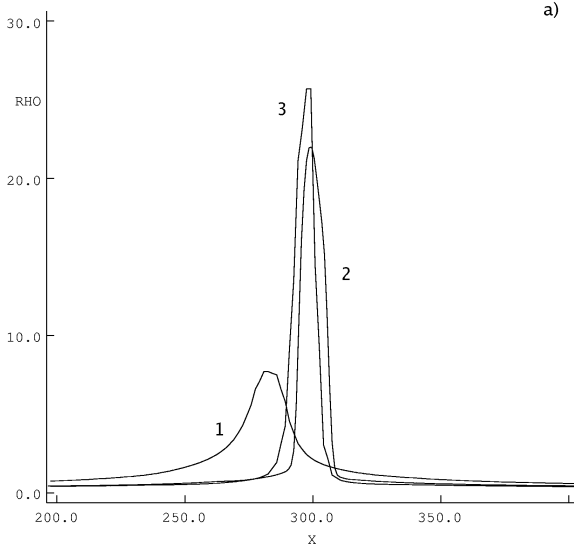


Figure 2. (a) The growth of the density perturbation at $y = 250$. The times are $t = 3 \times 10^3$, $2 - t = 3.5 \times 10^3$ and $3 - t = 3.6 \times 10^3$. (b) Decay of the density perturbation at $y = 250$. The times are $1 - t = 3.7 \times 10^3$, $2 - t = 4 \times 10^3$ and $3 - t = 4.5 \times 10^3$.

After 3 periods (i.e. $t \approx 3000$) the fast-mode steepens into a shock, thereby exciting slow-mode components. FH02 showed that these slow modes produce inhomogeneities with large density contrasts. Since there are as yet no significant variations in the y -direction, these high-density perturbations aligned with the y -axis. Figure 2 shows the growth of one such high-density region and its subsequent decay. Up to $t \approx 5000$, the maximum densities in the computational domain do not differ significantly from those in 1D (see Fig. 3). The density profiles of the perturbations are also similar to the 1D ones (see Fig. 2 and FH02).

We can also see from Fig. 2b that the density pertur-

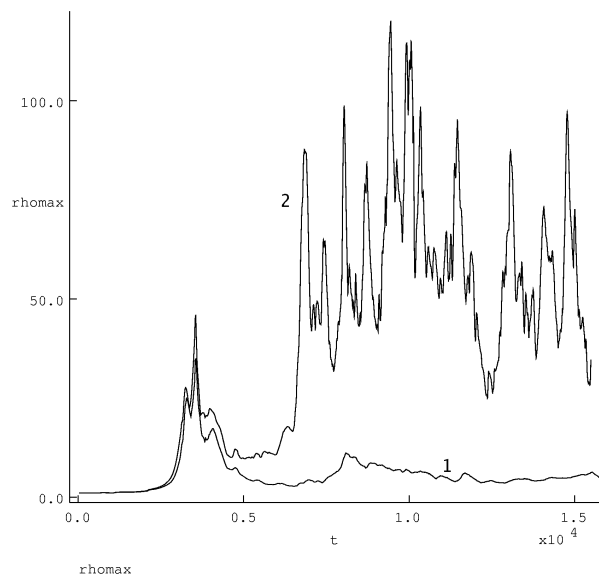


Figure 3. The maximum density measured in the computational domain for both 1D (1; from FH02) and 2D (2) as a function of time.

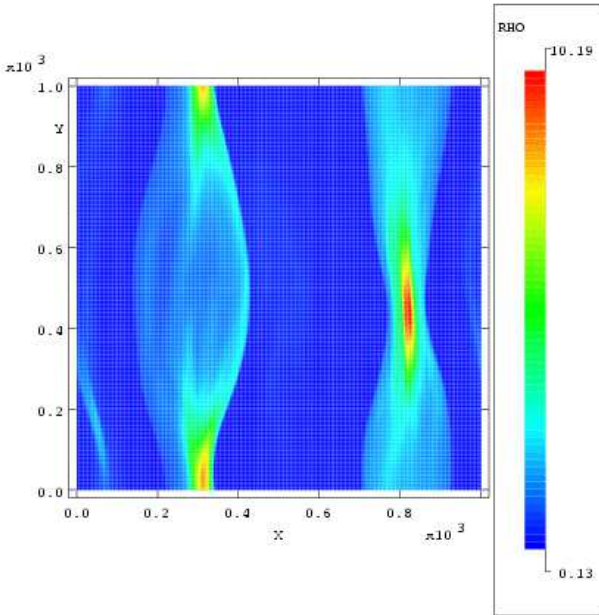


Figure 4. The density at $t = 5500$. The density perturbations are bounded by curved shocks. The density is highest in the central region where the shocks are moving slowly.

bation is bounded by shocks as it expands. In contrast to the 1D case, the speed in the laboratory frame, v_s , of these shocks is not constant along the shock front. The upstream fluid speed in the frame of the shock, v_u , is roughly constant and equal to $A_1 c_a$ (FH02), where $c_a = |B_x|/\rho^{1/2}$ is the initial Alfvén speed, whereas the upstream speed in the rest frame, v_p , varies considerably along the shock front. Since $v_s = v_p - v_u$, it follows that v_s must also vary along the

shock front i.e. the shock front is curved. This effect can be seen clearly in Fig. 4.

An important consequence of the curved shock front is the formation of clumps, rather than dense sheets. The dense regions are bounded by slow shocks that propagate predominantly in the x -direction. Regions that are bounded by slowly moving shocks therefore retain a high density for longer than those bounded by faster shocks. At later times this produces variations in the y -direction that are larger than those that occurred before the initial decay. However, there is little motion in the y -direction because this is prevented by the magnetic field. Once a clump forms, its long axes is orientated perpendicular to the magnetic field lines, but its aspect ratio is not particularly large (see Fig. 6).

Although the average density within clumps is nearly constant, the maximum density can have large fluctuations. As seen from Fig. 3, the maximum densities are a factor of two higher than obtained in 1D calculations. The initial fast-mode is still present and interacts with the clumps and its bounding shocks, thereby generating slow-mode waves. Figure 5 shows a measure of the amplitude of fast and slow-mode waves as defined in FH02. It shows clearly the correlation of the slow-mode waves with the density inhomogeneities. The slow modes are thus responsible for the fragmentation of the clump into high-density contrasts. Figure 6 shows a close-up of a clump with dense substructures. Such fragmentation is, of course, not possible in 1D.

The dense substructures in the clump are thus transient and have rather short lifetimes. They are generated because slow-mode waves are continuously excited by the fast-mode wave interacting with the clump. This explains why the time-scales of the density fluctuations are of the order of the time for a fast-mode wave to cross the computational domain, i.e. $t = 1000$. As this wave dissipates, the amplitude of the slow modes decreases, resulting in lower density contrasts (see Fig. 5). Furthermore, the clump itself disperses. The 2D results show that a clump persists for a period of time that exceeds the lifetimes of the density perturbations in 1D by a factor of 10.

The ratio, β , of the gas pressure to magnetic pressure increases in our simulations from its initial value of $\beta \approx 0.002$ to $\beta \approx 0.2$. While the gas pressure can become a factor of 100 larger than initially since it scales like the density, the magnetic field does not vary much in strength. When β approaches unity, the process of producing high-density contrasts by slow modes ceases to be effective. There is therefore an upper limit to the maximum density that can be produced.

4 PARAMETER STUDY

In the previous section, we focused on one specific numerical case with a set of specific parameters. As the results are parameter-dependent, we briefly discuss the influence of each parameter.

α : The fast-mode wave is most efficient in exciting slow-mode components for modest values of the angle, α , between its direction of propagation and the magnetic field (FH02). When α is too large, the shock is not effective in producing slow-mode components, whereas there is little steepening

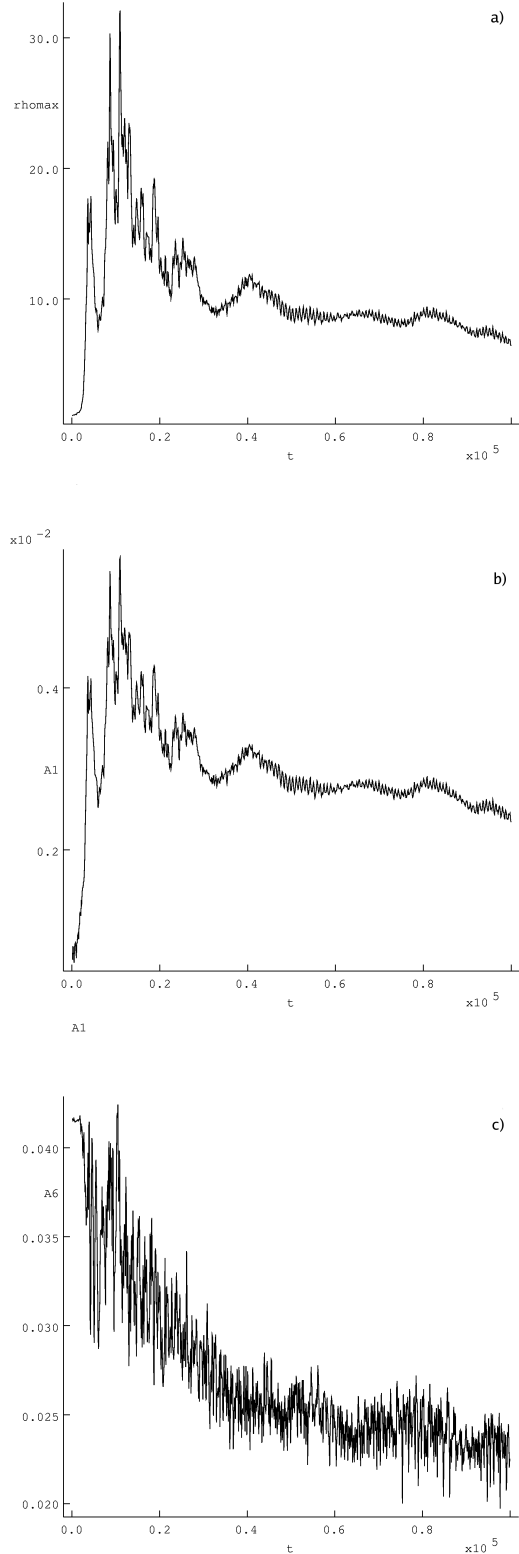


Figure 5. (a) Similar to Fig. 3, but now for a uniform grid with 100×100 mesh points up to $t = 100\,000$. (b) The maximum value for the amplitude-measure of the slow-mode wave in the computational domain (for definition see FH02). (c) Similar to (b), but for the fast-mode wave.

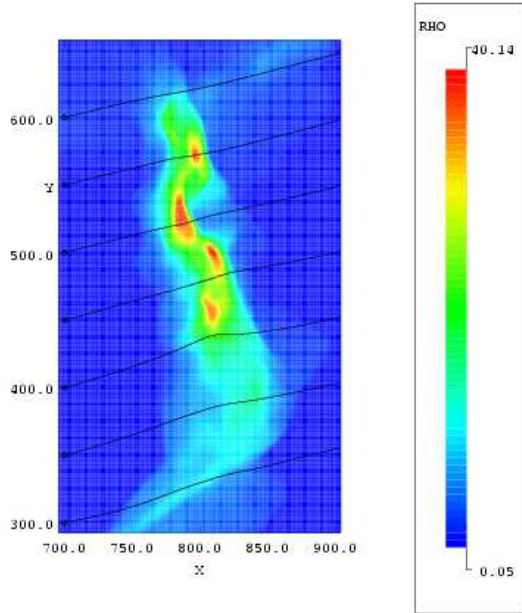


Figure 6. Hierarchical structure in the density at $t = 12000$: a number of dense cores reside in a larger clump. The magnetic field is represented by the solid lines.

ing when α is too small. Moreover, the fast-mode wave is also responsible for the excitation of slow modes within the clumps. Since it is the slow modes that generate the density inhomogeneities, this means that models with $\alpha \neq 0.25$ produce lower density contrasts.

A₁ and a : Both parameters affect the maximum density produced by the non-linear steepening of the fast-mode wave. FH02 showed that the maximum density is roughly proportional to A_1^2/a^2 .

While the time-scale for the formation of the substructure is independent of a , it depends on A_1 in two ways (see FH02). The wave amplitude determines the time for the fast-mode wave to steepen into a shock and also the time-scale for the subsequent decay. A lower value of A_1 means that dense cores arise later in the simulations.

A₂ : The phase-shift of the fast-mode wave is responsible for the variations along the y -axis. The amplitude of this shift determines the time at which the simulations cease to be 1D. Figure 7 shows the time evolution of the maximum density for an amplitude of $A_2 = 0.1$. As the initial variations are a factor of 10 smaller than for $A_2 = 1$, it takes longer to develop any significant deviation from 1D. This also means that the formation of substructure is deferred. Note that the maximum density that can be attained is independent of A_2 (see Fig. 3 and Fig. 7).

L₁ and L₂ : The wavelengths of the fast-mode wave and the phase shift determine the dimensions of the clump. Its extent in the x -direction is roughly comparable with the size of density perturbations produced by excitation of slow modes. This means that it is $\approx L_1 \rho_0 / \rho_{\max}$, where ρ_0 is the initial density and ρ_{\max} the maximum density. The size in the y -direction is set by the wavelength of the phase shift.

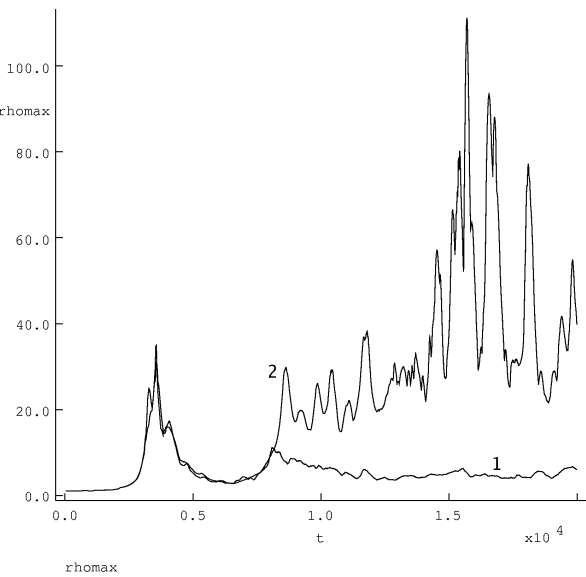


Figure 7. Similar to Fig. 3, but now for $A_2 = 0.1$.

As mentioned in Sect. 3, a sinusoidal phase shift divides the domain into two separate regions so that the y -extent is roughly $L_2/2$.

5 DISCUSSIONS AND CONCLUSIONS

We have extended the FH02 model which describes the generation of density inhomogeneities by MHD waves in a low- β environment, to two dimensions. We have followed the evolution of a fast-mode wave propagating in the positive x -direction with a small, but non-negligible, variation in the y -direction produced by a y -dependent shift along the x -axis. Like FH02, we find that the formation of density inhomogeneities is associated with the excitation of slow modes by the fast-mode wave.

An important result is that the process of generating structure by slow modes works on different length-scales. While the larger structures arise due to the non-linear steepening of the fast mode, there are smaller structures generated by the interaction between the fast-mode wave and the larger structures. A limiting factor, however, is that β increases within each level of substructure. When β approaches unity, the mechanism ceases to be effective and produces no further substructures. β is probably about unity in dense cores (e.g. Myers 1990).

Although we made no attempt at reproducing any observational data, we can investigate the relevance of our simulations to observations of clumps and dense cores in GMCs. The structure of molecular clouds is often described as filamentary or clumpy (e.g. Blitz & Williams 1997). For example, observations of the ρ Oph A core show an arc-shaped ridge with 4 embedded cores (André, Ward-Thompson & Barsony 1993). Similar structures are obtained in our simulations. However, the shape of the clump depends on the properties of the initial fast-mode wave, i.e. its wavelength, and on the length-scale of per-

pendicular variations (in our calculations determined by the sinusoidal phase-shift of the fast-mode wave). Other shapes of clumps can then be reproduced by MHD waves with different properties.

Blitz & Stark (1986) found that the clumps in the Rosette Molecular Cloud, an archetypal GMC, are an order of magnitude denser than the mean cloud density. Dense cores within the clumps typically have a density that exceeds the mean density by two orders of magnitude, but peak densities in pre-stellar cloud cores can range to values that exceed the mean density by 4 orders of magnitude (e.g. Larson 2003). In our simulations, we find that the average density contrasts in the larger structures are in excess of 10 times the average background density of 1. For the substructures, i.e. individual dense cores, this increases to 100. We do not find the observed peak values, but this can be readily explained by the fact that we have restricted ourselves to modest amplitudes of the initial fast-mode wave. Also we have not included self-gravity in our model. The inclusion of this effect will be investigated in a subsequent paper. However, we expect self-gravity only to act as an amplifier and not to have an influence on the fragmentation of the molecular cloud.

Recently, Garrod et al. (2005) investigated the chemistry of transient dense cores within molecular clouds. Using the results of FH02 to describe the growth and decay of the dense cores, they find a significant enhancement in chemical compositions of the cores as they disperse. This leads eventually to chemical enrichment of the molecular cloud. In our simulations, however, high-density clumps survive much longer than they do in FH02. Our results thus have serious implications for the chemical evolution and richness of clumps and dense cores.

ACKNOWLEDGMENTS

We thank the anonymous referee for a report that helped to improve the manuscript. SVL gratefully acknowledges PPARC for the financial support.

REFERENCES

André P., Ward-Thompson D., Barsony M., 1993, *ApJ*, 406, 122

Ballesteros-Paredes J., MacLow M.-M., 2002, *ApJ*, 570, 734

Blitz L., Stark A. A., 1986, *ApJ*, 300, L89

Blitz L., Williams J. P., 1997, *ApJ*, 488, L145

Crutcher R.M., 1999, *ApJ*, 520, 706

Dedner A., Kemm F., Kröner D., Munz C.-D., Schnitzer T., Wesenberg M., 2002, *JCP*, 175, 645

Falle S. A. E. G., Hartquist T. W., 2002, *MNRAS*, 329, 195

Falle S. A. E. G., Komissarov S. S., 2001, *J. Plasma Phys.*, 65, 29

Falle S. A. E. G., Komissarov S. S., Joarder P., 1998, *MNRAS*, 297, 265

Gammie C. F., Lin Y.-T., Stone J. M., Ostriker E. C., 2003, *ApJ*, 592, 203

Garrod R. T., Williams D. A., Hartquist T. W., Rawlings J. M. C., Viti S., 2005, *MNRAS*, 362, 749

Larson R. B., 2003, *RPPh* 66, 1651

Li P. S., Norman M. L., MacLow M.-M., Heitsch F., 2004, *ApJ*, 605, 800

Lim A. J., Falle S. A. E. G., Hartquist T. W., 2005, *MNRAS*, 357, 461

Myers P. C., 1990 in T. W. Hartquist, ed., *Molecular Astrophysics – A volume honouring Alexander Dalgarno*. Cambridge University Press, Cambridge, p. 328

Nakamura F., Li Z.-Y., 2005, *ApJ*, 631, 411

Padaan P., Nordlund A., 2002, *ApJ*, 576, 870

Vázquez-Semadeni E., Kim J., Shadmehri M., Ballesteros-Paredes J., 2005, *ApJ*, 618, 344